CRYSTAL GROWTH & DESIGN

Article

A Breathing Metal-Organic Framework Based on Flexible Inorganic Building Units

Erik Svensson Grape, Hongyi Xu, Ocean Cheung, Marion Calmels, Jingjing Zhao, Catherine Dejoie, Davide M. Proserpio, Xiaodong Zou, and A. Ken Inge

Cryst. Growth Des., **Just Accepted Manuscript** • DOI: 10.1021/acs.cgd.9b01266 • Publication Date (Web): 03 Dec 2019

A Breathing Metal-Organic Framework Based on Flexible Inorganic Building Units

Erik Svensson Grape,[†] Hongyi Xu,[†] Ocean Cheung,[‡] Marion Calmels,[§] Jingjing Zhao,[†] Catherine Dejoie,[⊥] Davide M. Proserpio,[∥,▽] Xiaodong Zou,[†] A. Ken Inge*[,†]

[†]Department of Materials and Environmental Chemistry, Stockholm University, SE 106 91 Stockholm, Sweden

[‡]Division of Nanotechnology and Functional Materials, Department of Engineering Sciences, The Ångström Laboratory, Uppsala University, Box 534, SE-751 21 Uppsala, Sweden

[§]INSA Lyon – Département Sciences et Génie Des Matériaux, 69621 Villeurbanne Cedex, France

[⊥]ESRF – the European Synchrotron Radiation Facility, CS40220, Grenoble 38043, France

[∥]Dipartimento di Chimica, Università degli Studi di Milano, Milano, 20133, Italy

[▽]Samara Center for Theoretical Materials Science (SCTMS), Samara State Technical University, Samara 443100, Russia

ABSTRACT: Five novel bismuth carboxylate coordination polymers were synthesized from biphenyl-3,4′,5-tricarboxylic acid (H_3BPT) and [1,1′:4′,1′′]terphenyl-3,3′′,5,5′′-tetracarboxylic acid (H_4TPTC). One of the phases, [Bi(BPT)]·2MeOH (denoted SU-100, as synthesized), is the first example, to the best of our knowledge, of a reversibly flexible bismuth-based metal-organic framework (MOF). The material exhibits continuous changes to its unit cell parameters and pore shape depending on the solvent it is immersed in and the dryness of the sample. Typically, in breathing carboxylate-based MOFs, flexibility occurs through tilting of the organic linkers without significantly altering the coordination environment around the cation. In contrast to this, the continuous breathing mechanism in SU-100 involves significant changes to bond angles within the Bi_2O_{12} inorganic building unit (IBU). The flexibility of the IBU of SU-100 reflects the non-discrete coordination geometry of the bismuth cation. A disproportionate increase in the solvent accessible void volume was observed when compared to the expansion of the unit cell volume of SU-100. Additionally, activated SU-100 (SU-100-HT) exhibits a large increase in unit cell volume, yet has the smallest void volume of all the studied samples.

Introduction

Metal-organic frameworks (MOFs) are porous three-dimensional framework structures formed by joining polytopic linker ligands with cationic metal centers. MOFs commonly exhibit very high porosity and large internal surface areas, and show promise in a wide range of applications, such as gas storage and catalysis.[1]

A subset of MOFs exhibit remarkable framework flexibility without altering their topology.[2–4] The "breathing" of these MOF structures (i.e. the reversible expansion and contraction of the pores) is often dictated by host-guest interactions. Potential uses of breathing MOFs lie in controlled release of guest species or increased selectivity in their absorption properties.[5] This structural flexibility has been described systematically in different ways.[2–5] In one sense, framework flexibility can be described to occur in one, two or three dimensions, or alternatively, as a consequence of two-, one-, and zero-dimensional rigidity of the framework.[3]

For cations with a well-defined coordination geometry, the flexibility of the framework can often be found to originate in the tilting of the organic linkers, yielding a corresponding change in the shape of the framework.

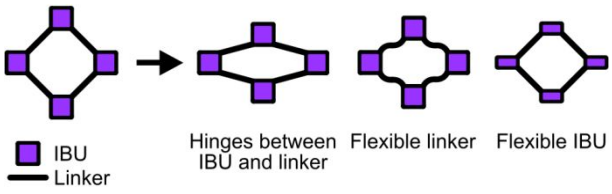

Figure 1. Selected examples of flexibility modes for MOFs, where the flexibility may originate from the presence of hinges between the linker and the metal cation, or alternatively from deformations of the linker or inorganic building unit, as described in this work.

Alternatively, the transformation can be caused by a shifting of interpenetrated frameworks, giving three-dimensional flexibility despite an apparent three-dimensional rigidity for the individual frameworks, yet, this article will focus on non-interpenetrated frameworks.

As described by Férey and Serre[4], flexibility can be found to follow a set of empirical rules, related to the framework topology, the linker connectivity, and the inorganic building units (IBUs) present in the structure. One archetypical example of a flexible MOF is the trivalent metal terephthalate MIL-53, which shows a decrease in unit cell volume of 32 % upon adsorption of water.[6]

This effect comes from the coordinating carboxylate groups acting as hinges (shown schematically in Figure 1), allowing a large change in shape of the rhombohedral channels of the structure. Structural changes of this nature were further described by Sarkisov *et al.*, summarizing that the functional groups, such as carboxylate groups, of the linkers create "weak points", thereby allowing a rearrangement of the structure.[7] The role of cations for the flexibility of MOFs has been studied as well, where breathing effects have been found to originate in a change of coordination environment for the cation through, for example, the loss of coordinated solvent molecules.[2,8,9] Additionally, the choice of cation has been found to play a role in the temperature-dependent threshold behavior for a narrow-pore to large-pore transition of an isostructural series of flexible MOFs[10], where the choice of cation was also found to affect the magnitude of the volumetric changes observed.

Only a relatively small number of MOFs have been published using Bi^{3+}, which is the heaviest of the stable post-transition metals.[11] Complexes of Bi^{3+} often show a high coordination number (typically 6-10) and regularly form infinite IBUs, i.e. rods and layers. In contrast to the thousands of MOFs which have been published so far, only five porous bismuth-containing MOFs (Bi-MOFs) have to the best of our knowledge been reported to possess 3D framework structures while also exhibiting a Type I sorption isotherm towards nitrogen.[12–16] The challenge in making porous bismuth materials seems to be that bismuth coordination polymers tend to form dense phases, a consequence of the fluidity in coordination environment around the Bi^{3+} cations, in contrast to the more well-defined coordination geometries of the transition metals and lighter cations. Bismuth is also interesting from a biological point of view, as it is considered non-toxic and has been shown to possess antibacterial and antitumoral activity, as well as to aid in the treatment of multi-resistant bacterial strains.[17–21] As such, one potential application of Bi-MOFs is as drug delivery carriers, but also as stand-alone active pharmaceutical ingredients.

The five porous Bi-MOFs published so far are, in chronological order, CAU-7[12], NOTT-220[13], CAU-17[14], CAU-33[15], and Bi-NU-901.[16] The synthesis of the materials was reportedly carried out under solvothermal conditions, and the most consistently used solvents were methanol and N, N-dimethylformamide (DMF), or mixtures thereof with other solvents and additives. The linkers used were all carboxylates with aromatic rings and the coordination number for the bismuth cation in the structures range from 6-9, with Bi-O distances of 2.2-3.0 Å. The aforementioned fluidity in coordination geometry of Bi^{3+} can give rise to very intricate structures and new topologies, most notably seen in CAU-17, where Bi^{3+} and trimesate ions form an arrangement of helical Bi-O rods which gives a previously unseen topological complexity.[14]

As a consequence of the often micro- or nano-crystalline nature of bismuth-containing coordination polymers, structure determination by conventional single-crystal X-ray diffraction (SCXRD) methods is seldom possible. In several cases, such as CAU-7, CAU-31 and bismuth subgallate[22], 3D electron diffraction (ED) using a transmission electron microscope (TEM) proved to be a very useful tool in order to acquire an initial structure solution from single micro- or nano-sized crystals. The possibility of fast 3D ED data collection, which requires only a few seconds or minutes of sample exposure to the electron beam (recently made possible by modern detectors), allows for the characterization of materials which were previously considered too beam sensitive.[22–26] However, due to dynamic effects, the 3D ED data often have high R-values compared to X-ray data. Therefore, structural models acquired from 3D ED data are often refined against X-ray powder diffraction (XRPD) data.

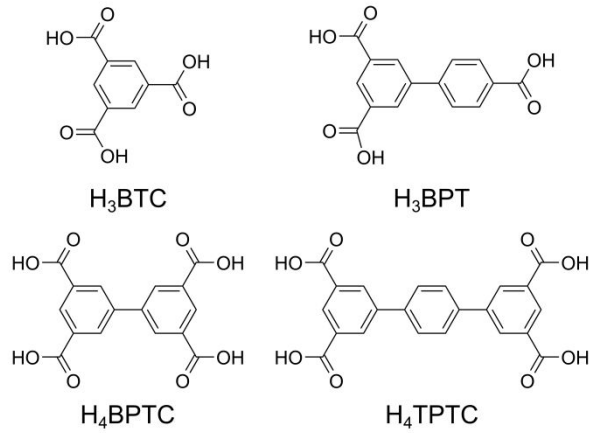

Figure 2. Linkers used for CAU-17 (H_3BTC) and NOTT-220 (H_4BPTC). The molecules to the right are the corresponding extended versions of the two previously used linkers: biphenyl-3,4′,5-tricarboxylic acid (H_3BPT) and [1,1′:4′,1′′]terphenyl-3,3′′,5,5′′-tetracarboxylic acid (H_4TPTC).

Considering the synthetic routes of the frameworks previously published, two specific linker molecules were chosen for the work described in this article: H_3BPT (biphenyl-3,4′,5-tricarboxylic acid) and H_4TPTC ([1,1′:4′,1′′]terphenyl-3,3′′,5,5′′-tetracarboxylic acid) (Figure 2). Both of these linkers can be considered as

extended versions of linkers that have been used for the synthesis of Bi-MOFs (CAU-17 and NOTT-220 respectively). Herein, we report the synthesis of five novel bismuth-containing coordination polymers, where one proved to be a breathing Bi-MOF containing a flexible IBU which undergoes continuous changes to the unit cell volume as a response to solvent and dryness. Structure determination of the five phases was performed using a variety of crystallographic techniques. For sufficiently large crystals, routine structure determination was performed with SCXRD data. The structures of phases that could only be synthesized as micro- or nano-crystalline powders were solved using the continuous rotation electron diffraction (cRED) method (one of the 3D ED techniques, such as ADT[27,28] and MicroED[24,29]) and subsequently refined against XRPD data. The novel structures were subsequently subjected to topological analysis in order to acquire insights into the connectivity of the frameworks.

Results and discussion

Through varying the linker, solvent (water or methanol), synthesis time, and bismuth-to-linker ratio, five coordination polymers were acquired (Figure S1). The initial ambition was to acquire isoreticular structures, in this case of CAU-17 and NOTT-220, which proved to be difficult. Each of the five structures synthesized are described in the subsections that follow.

Crystal Structure of Bi(BPT)•2MeOH (SU-100)

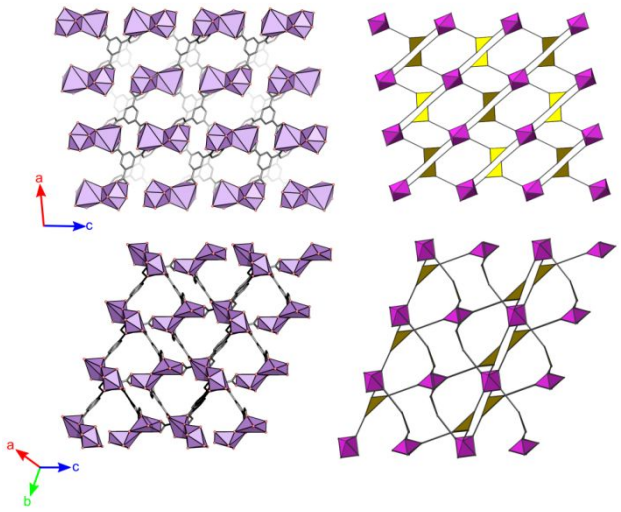

Figure 3. Views along [010] (top) and [111] (bottom) for Bi(BPT)•2MeOH (SU-100, as synthesized) (left) and the corresponding augmented **esg** net (right). Solvent molecules have been omitted for clarity. In the augmented net representations, three-coordinated linker molecules are represented as yellow triangles, and the bismuth dimers as distorted octahedra (in purple).

The metal-organic framework, Bi(BPT)•2MeOH (SU-100 (**1**), as synthesized), was acquired through synthesis in methanol under solvothermal conditions, as aggregates of plate-shaped crystals (0.8 x 0.3 x 0.01 μm³, Figure S2). The structure (Figure 3) was solved from cRED data (Figure 4) and refined against high-resolution XRPD data (Figure S3-S4, Table S1-S2).

The IBU of SU-100 is a Bi_2O_{12} dimer, where each Bi^{3+} cation has a coordination number of 7, and two of the oxygen atoms bridge the two Bi^{3+} in an edge-sharing manner. The asymmetric unit comprises one Bi^{3+} and one BPT^{3-}. Thus, the two Bi^{3+} in the dimer are related by symmetry. The Bi-O bond distances in SU-100 range from 2.3 to 2.7 Å, which is in good agreement with previously published structures. Each of the Bi^{3+} ions is chelated by three carboxylate groups resulting in the six shorter Bi-O bonds (2.3-2.6 Å). The seventh and longest Bi-O bond (2.7 Å) involves an oxygen atom from a carboxylate that chelates to the other Bi^{3+} in the dimer. The coordination geometry of the Bi^{3+} centers are that of an irregular decahedron, with one face pointing towards the pores being seemingly empty when assessing the structure solution from cRED data. However, refinement against high-resolution XRPD data suggested a coordinated methanol molecule in the open site (Bi-O distance of ~ 2.8 Å) for both the as-synthesized and methanol-soaked sample, with additional methanol molecules residing in the pores of the structure. The discrepancy in the occupancy of the coordinating methanol in the models generated from cRED data and the XRPD data is attributed to the removal of methanol under the ultra-high vacuum inside the TEM. The framework has two kinds of channels of similar diameter (7-8 Å), one along the *b*-axis and another along the [111] diagonal of the unit cell (Figure 3). The channels intersect with each other, resulting in a two-dimensional channel system (Figure S8). A topological analysis of the framework shows two kinds of nodes making up a (3,6)-c net. The tricarboxylate linker is represented as the 3-coordinated node, while the IBU is represented as the 6-coordinated node, shown as yellow triangles and distorted octahedra, respectively, in Figure 3. The net, for which the point symbol is $\{4.8^2\}_2\{4^2.8^{12}.10\}$, has been assigned the symbol **esg**, in the Reticular Chemistry Structure Resource (RCSR) database.[30] Additionally, the net shows a tiling with two kinds of tile (Figure S7), having a transitivity of 2352. The net has been found in previously described structures and has since been given the ToposPro name alb-3,6-C2/c, being a subnet of **alb**.[31,32] When using the

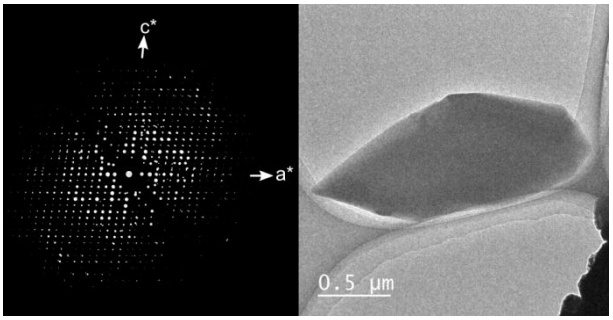

Figure 4. Reciprocal space projection for 3D ED data (viewed

along b*) acquired for SU-100 (left) as well as the crystal studied (right).

standard simplification method in ToposPro, a 4,4-coordinated net can be found (wherein the IBU is treated as two 4-coordinated nodes). The net found is a subnet of **roa**, and has been seen observed in MOFs built from similar linkers.[33]

Flexibility of SU-100

The idea that SU-100 might be a flexible framework arose upon observing significantly different diffractograms when recollecting XRPD data on a previously characterized sample, showing an apparent change in unit cell parameters. The effect was then systematically investigated by exposing the as-synthesized SU-100 (stored for more than one week in air) to different solvents (methanol [MeOH], N,N-dimethylformamide [DMF], N,N-diethylformamide [DEF]) and subsequently gathering high-resolution XRPD for three of the samples (as-synthesized SU-100, MeOH@SU-100, and DEF@SU-100).

Extended flexibility could be observed when exposing SU-100 to DMF or DEF, resulting in unit cell volumes of 3841 Å^3 and 3954 Å^3, respectively. Compared to the as-synthesized state (3584 Å^3, Figure 5, Table S2), this corresponds to a relative increase in unit cell volume of 10.2 %. This solvent-dependent swelling effect is reversible and SU-100 reverts to a cell-volume close to the as-synthesized stage upon storage, shrinking from 3954 Å^3 (heated in DEF, 100 °C for one hour, Table S4) to approximately 3600 Å^3 when left at an elevated temperature (140 °C, in air) overnight. The structure then re-expands to a cell volume of approximately 3800-3900 Å^3 when adding a few drops of methanol or isopropanol to the powder.

The mechanism of structural flexibility was investigated by comparing the crystal structures of as-synthesized SU-100, MeOH@SU-100 and DEF@SU-100, which were refined against high-resolution synchrotron XRPD data (Figure S4-S6, Table S2-S4). In contrast to the common modes of flexibility described in literature, the breathing of SU-100 is largely attributed to changes in the coordination geometry of the bismuth cation, giving rise to a three-dimensional framework flexibility (see video in Supporting Information, Web Enhanced Object). The most notable change is that of the bond angles involving the bridging oxygen atoms and the Bi^{3+} cations in the bismuth dimer (Figure 6). This fluidity in coordination geometry, and hence the overall shape of the IBU, most likely originates in the ill-defined coordination geometry of Bi^{3+}. The overall breathing effect is possibly also promoted by the rhombus-shaped rings within the IBU as well as between several building units of the structure (Figure 3) which can expand and contract.

One change that can be observed is that the Bi-O-Bi angles decrease from 121.1(5)° to 110.5(3)°, leading to a shortening of the Bi···Bi distance in the dimer from 4.608(2) Å to 4.433(2) Å, in as-synthesized SU-100 and DEF@SU-100, respectively. The two bridging carboxylate groups are significantly closer to one another in the as-synthesized SU-100, with a C···C distance of 4.32(1) Å, in comparison to DEF@SU-100, where the respective C···C distance is noticeably longer at 5.060(9) Å. Additionally, the inorganic building unit is rotated in relation to the rest of the structure, where the angle between the plane formed by the two bismuth atoms and the carboxylate carbons (connected to the bridging oxygen) with respect to the [100] direction changes from 27.5(1)° to 20.0(1)°. Both of these changes lead to an overall increase in the unit cell volume of SU-100.

The diffractograms show the largest changes when exposed to bulky solvent molecules. Apart from the increase in cell volume upon exposure to different solvents, the volume of solvent accessible voids (as determined by Platon's *Calc Solv*)[34] for the SU-100 framework also increases relative to the total unit cell volume, increasing from 35.2 % (1264 Å^3, as synthesized SU-100) to 38.1 % (1445 Å^3, MeOH@SU-100) and 40.4 % (1596 Å^3, DEF@SU-100). This 332 Å^3 increase of solvent accessible voids corresponds to a relative increase in void volume of 26 %, i.e. a disproportionately large change compared to the change in unit cell volume alone (solvent accessible voids are visualized in Figure S8). As such, the adsorption of DEF results in both a swelling of the lattice, as well as a change in pore shape in order to accommodate a larger solvent volume. Stability in other organic solvents and water (Figure S20) was confirmed by XRPD and N_2 adsorption (Figures S10, S15-S16).

Figure 5. Acquired X-ray powder diffractograms (left) as well as the unit cell volumes (right) of SU-100 (red), MeOH@SU-100 (blue), DMF@SU-100 (orange), and DEF@SU-100 (green). Data are plotted against d rather than 2θ, since they were collected at different

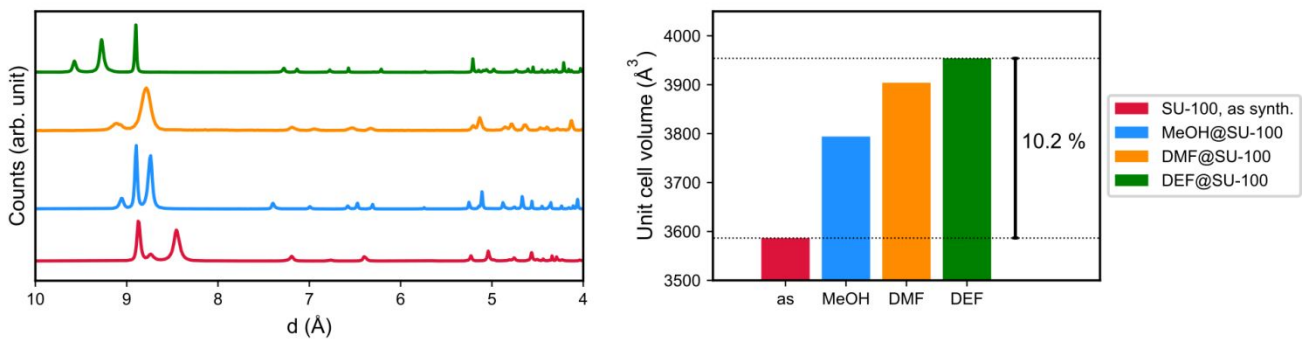

synchrotron beamlines utilizing X-rays of differing wavelengths. A unit cell volume increase of 10.2 % can be observed when comparing the as-synthesized SU-100 and DEF@SU-100.

To assess the thermal stability of SU-100, thermodiffraction data were gathered on as-synthesized material, showing that in air SU-100 first undergoes structural changes at 150 °C, followed by a loss of crystallinity at 350 °C (Figure S17). Similar structural changes occur when heating the sample under vacuum (Figure S18). The initial structural change is in part reversible, as a sample that had been heated to 250 °C under vacuum could be partially transformed back to the original material by cooling to room temperature and adding a few drops of isopropanol (Figure S18-S19). Additional reflections were observed in the XRPD data, suggesting the formation a phase mixture, however the structure of the minor phase that had formed was not identified. To investigate the changes that occur after heating SU-100, cRED data were collected on a sample (SU-100-HT, Table S5) which had been heated in air at 200 °C for 3 hours and then cooled down to room temperature prior to being put into the high-vacuum environment of the TEM. The crystal structure of SU-100-HT has an even larger unit cell volume of 4373 Å^3 (Table S5), corresponding to an increase of 22 % with respect the as-synthesized SU-100. The void volume, on the other hand, is only 21 % of the unit cell volume (917 Å^3) and the Bi-Bi distance in the Bi_2O_{12} dimer is 4.8 Å. As such, the void volume of SU-100-HT is smaller than that of the as-synthesized SU-100 (1264 Å^3 vs. 917 Å^3), despite having the largest unit cell volume. A plot of Bi-Bi distance vs. void volume can be seen in Figure S9, showing an inverse relationship between the two quantities.

Gas sorption properties of SU-100

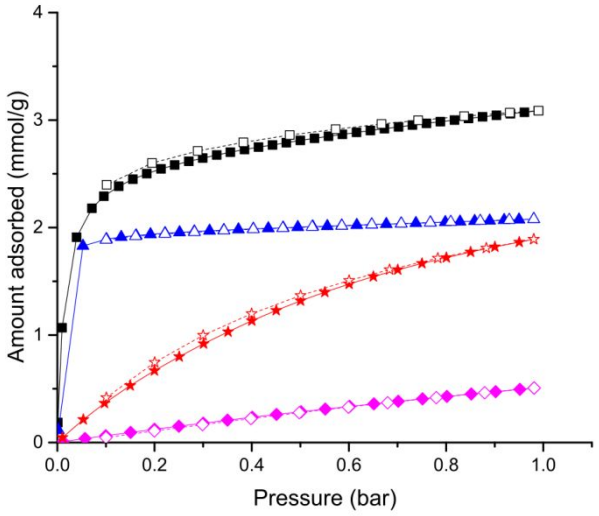

Figure 7. CO_2(black), SF_6 (blue), N_2 (purple), and CH_4 (red) adsorption/desorption isotherms of SU-100 recorded at 0 °C. The adsorption points are shown as solid symbols and the desorption points are shown as hollow symbols.

The gas adsorption properties of SU-100 were measured for numerous gases (N_2, CO_2, NO, SF_6). The N_2 adsorption/desorption isotherm of SU-100 is shown in Figure S10. The framework proved to be a microporous structure, exhibiting a Type I sorption isotherm for N_2. The average pore size of SU-100 was around 7 Å, according to the pore size distribution calculated using the density functional theory (DFT) method with an N_2 slit pore model (Figure S11).

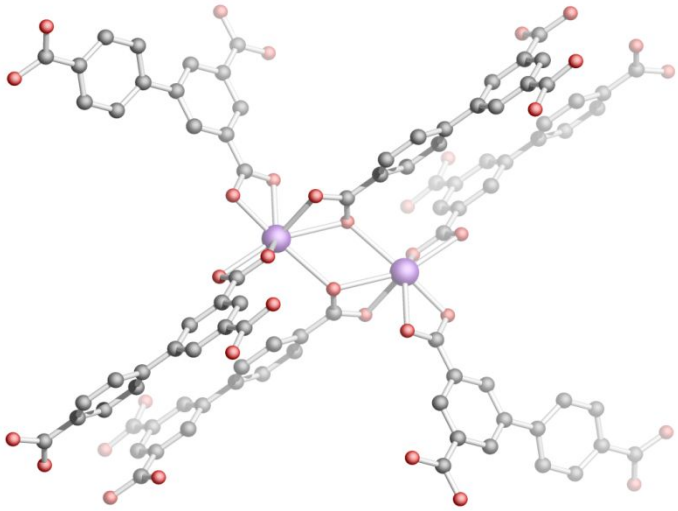

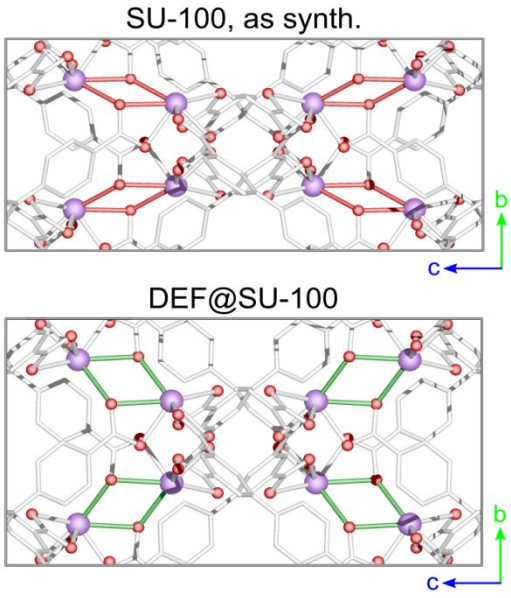

Figure 6. The bismuth dimer of SU-100, showing three BPT^{3-} coordinated to each Bi^{3+} (left) and the unit cells of as synthesized SU-100 (as synthesized) and DEF@SU-100 along [100] (right). The Bi-O bonds involving the bridging oxygen atoms are colored red (as-synthesized SU-100) and green (DEF@SU-100) to highlight changes in the IBUs.

Significant porosity was detected on SU-100 as indicated by a steep increase on the isotherm at low relative pressure. The shape of the isotherm is typical of a microporous material with uniformly shaped pores. The specific surface area of SU-100 was calculated to be 473 $m^2 g^{-1}$ using the Langmuir theory (BET surface area = 385 $m^2 g^{-1}$). SU-100 which had been exposed to water or toluene (100 °C for 1 hour) showed specific surface areas of 484 $m^2 g^{-1}$ and 482 $m^2 g^{-1}$, respectively, using the Langmuir theory (with corresponding BET surface areas of 395 $m^2 g^{-1}$ and 393 $m^2 g^{-1}$). This pore size is in good agreement with that acquired from the crystallographic model (7-8 Å). The functionality of the pores on SU-100 was tested by gas adsorption. SU-100 showed the ability to separate CO_2 from other gases, which is a desirable property in various applications such as carbon dioxide capture from exhausts of fossil fuel combustion (flue gas), as well as bio-gas upgrading. Figure S6 shows the CO_2, N_2, SF_6, and CH_4 adsorption/desorption isotherms of SU-100 recorded at 0° C. The CO_2 uptake of SU-100 reached 3.09 mmol/g at 1 bar, which was comparable to zeolites[35,36] and many other typical MOF materials.[22,37] CO_2 was preferentially adsorbed over N_2 and CH_4 under these conditions, as the uptake of N_2 and CH_4 at 1 bar was only 0.51 mmol/g and 1.89 mmol/g. The preferential uptake of CO_2 on SU-100 was related to the high quadrupole moment of CO_2 as well as its high polarizability when compared with N_2 and CH_4. Note that no hysteresis was observed for any of the recorded adsorption/desorption isotherms, confirming that these gases physisorbed on the surface of SU-100 with no chemisorption interaction. Using the initial slope method (applied to the Henry's law region of the isotherms) the CO_2/N_2 selectivity was found to be ~ 65. The CO_2/N_2 selectivity for a hypothetical fuel gas mixture that contains 15 kPa CO_2 and 85 kPa N2, and CO_2/CH_4 selectivity for a hypothetical biogas mixture that contains 50 kPa CO_2 and 50 kPa CH_4, were estimated using the equation s = (q1/q2)/(p1/p2). The CO_2/N_2 selectivity was 30.8 and the CO_2/CH_4 selectivity was 2.15 for these gas mixtures. The CO_2/N_2 selectivity was high, although other existing sorbents such as zeolite A[38,39] and (silico)-aluminophosphates[38,40] offer higher selectivity and higher CO_2 uptake under similar conditions. The heat of CO_2 adsorption on SU-100 was around 45-55 kJ/mol, depending on loading (see Supplementary Information, page S10, for details). These values appear to be higher than those of typical physisorbents for CO_2, which could be related to the narrow pore size of SU-100, being in a similar dimension as the CO_2 molecules. The slight increase in the heat of CO_2 adsorption at moderate loading (above 2 mmol/g) may be related to the flexible structure of SU-100, although further studies are required to fully understand this phenomenon.

SU-100 also showed preferential SF_6 uptake over N_2. SF_6 separation from N_2 is useful for various industries, particularly in the electronics manufacturing sector.[41,42] The SF_6 uptake on SU-100 reached 2.07 mmol/g at 1 bar (0 °C). The SF_6 isotherm showed a sharp increase at the low pressure range, suggesting that there is increased interaction between SF_6 and the pore surface of SU-100. On the other hand, the lack of a hysteresis loop showed that SF_6 physisorbed on SU-100. The increased physisorption interaction may be related to the average pore size (~0.7 nm) being in a similar dimension as the kinetic diameter of SF_6 (0.55 nm). The SF_6/N_2 selectivity for a gas mixture containing 90 kPa SF_6 and 10 kPa N_2 was 35.9.

Crystal Structure of $Bi_2O_2(HBPT)$ (2)

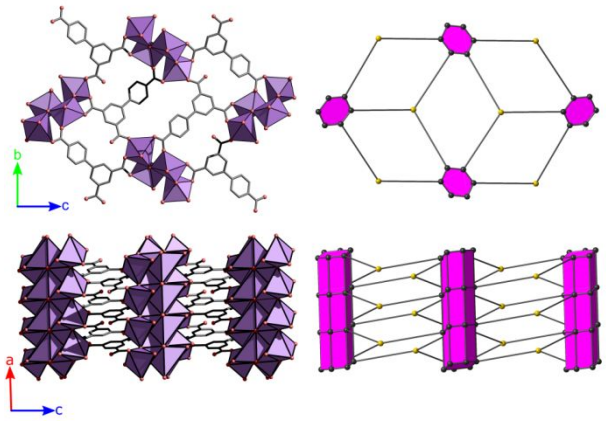

Figure 8. View along the *a*-axis for **2** (top left) and the corresponding net (top right) along the same viewing direction, as well as similar representations viewed along *b* (bottom). The three-coordinated and five-coordinated nodes in the net are shown as yellow and black spheres, respectively. The volume enclosed by the nodes originating from the IBU has been colored purple to highlight the different parts of the structure.

While SU-100 was synthesized under solvothermal conditions by combining $Bi(NO_3)_3 \cdot 5H_2O$ and H_3BPT in MeOH, three other bismuth coordination polymers were synthesized using water as the solvent instead (for an overview of the syntheses, see Figure S1). $Bi_2O_2(HBPT)$ (**2**) was acquired as needle-shaped crystals (Figure S22) when employing relatively short reaction times (two to four hours). After longer synthesis times, **2** transforms into a mixture of $Bi(OH)(H_2BPT)_2(H2O)_2 \cdot H_2O$ (**3**) and $Bi_2(HBPT)_3(H_2O)_3 \cdot H_3BPT$ (**4**). The structure of **2** was solved using cRED (Figure S23, Table S6) and later refined against high-resolution synchrotron XRPD data (Figure S24, Table S7). The crystal structure of **2** proved to be a dense coordination polymer, as seen in Figure 8.

The coordination numbers for two independent Bi^{3+} cations in **2** is six and seven, forming distorted octahedra and distorted pentagonal bipyramids, respectively, where the Bi-O bond distances range from 2.15-2.75 Å. The IBU

consists of Bi rods, linked together by six BPT^{3-} molecules for each sequence of the rod. For the topological analysis, the bismuth rods were represented by taking the point of extension of the linker (the carboxylate carbons) and linking them together, as described by Rosi *et al.*[43], giving a hexagonal prism. For the organic part of the structure, there are two apparent choices: if the linker is represented as a single three-connected node, **2** is found to form a 3,5,5-c net with a stoichiometry of (3-c)(5-c)$_2$(5-c) and a point symbol of $\{4^4.6^4.7^2\}\{4^4.6^5.7\}_2\{6^3\}$. The tiling found for this net has a transitivity of 3685 (Figure S25). Alternatively, if the linker is represented as three individual 3-c nodes, representing the branch points of the linker, **2** is found to form a 3,3,5,5-c net with ratios of (3-c)(3-c)(5-c)(5-c)$_2$. The point symbol for the acquired net is then $\{3.8^2\}_3\{4^4.6^2.8^2.9^2\}\{4^4.6^2.8^3.9\}_2$. This net can also be described by a natural tiling and has a transitivity of 6(12)(13)7, i.e. seven tiles (Figure S61).

Crystal Structure of $Bi(OH)(H_2BPT)_2(H_2O)_2 \cdot H_2O$ (3)

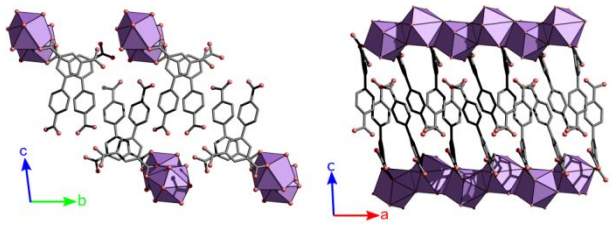

Figure 9. The structure of **3**, as viewed along the *a*-direction (left) as well as the *b*-direction (right). The inorganic building units of the structure are bismuth rods, which are not linked together, but rather held together through hydrogen bonding and π-π-stacking between H_2BPT molecules. Hydrogen atoms have been omitted for clarity.

Another one of the aforementioned dense phases, which forms after extended synthesis times in water when using a Bi^{3+} to H_3BPT ratio of 2:1, is $Bi(OH)(H_2BPT)_2(H_2O)_2 \cdot H_2O$ (**3**). The bladed crystals of **3** (Figure S27) were acquired selectively when using an excess of linker with respect to Bi^{3+}. The structure was solved using SCXRD (Table S8). The structure is a one-dimensional coordination polymer (Figure 9), where hydrogen bonding and π-π-stacking join the rods together (hydrogen bonds are shown in Figure S28). The IBU of the structure is a bismuth-oxo rod, where each Bi^{3+} cation is coordinated by two bridging carboxylates from the H_2BPT molecules, two terminal water molecules, and two μ_2-hydroxide ions. The coordination number for bismuth in **3** is eight, and Bi-O bond distances range from 2.2 up to 2.9 Å.

Crystal Structure of $Bi_2(HBPT)_3(H_2O)_3 \cdot H_3BPT$ (4)

When using a one-to-one ratio between bismuth and H_3BPT during synthesis in water for extended periods of time, large prismatic crystals of a dense phase, $Bi_2(HBPT)_3(H_2O)_3 \cdot H_3BPT$ (**4**) (Figure S30), were acquired as the main product. The structure of this three-dimensional coordination polymer was solved and refined in *P*1 as a racemic twin (3:2 ratio, Table S9), and, as seen in Figure 10, the non-centrosymmetric structure would be porous were it not for the non-coordinating H_3BPT molecule trapped within the voids of the framework, which forms one-dimensional channels along $[0\bar{1}1]$. This non-coordinating molecule is held in place through π-π interactions with the framework. As such, the non-coordinated molecule may act as an organic structure-directing agent (OSDA) for the structure of **4** in a form of self-templating. The IBU in **4** is a bismuth dimer, linked together by two- and three-coordinated $HBPT^{2-}$ ions. The coordination number for bismuth in **4** is six and seven, respectively, where one of the cations is coordinated to two terminal water molecules rather than one. The Bi-O distances in the structure range between 2.2-2.9 Å. The two three-coordinated linker molecules were represented as three-coordinated nodes, whereas the two-coordinated $HBPT^{2-}$ molecule is represented by an edge between the eight-coordinated nodes representing the bismuth dimer. A topological analysis of this (3,3,8)-c net gives a point symbol of $\{4^3\}_2\{4^6.6^{18}.8^4\}$ and the net is **tfz-d** (the high-symmetry form of the net has the space group *P*6/*mmm*). It forms a natural tiling with transitivity 2222.

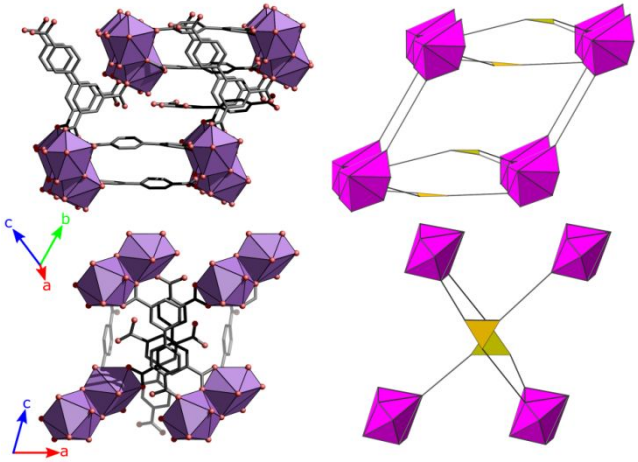

Figure 10. View along the *a*-axis for **4** (top left) and the corresponding augmented net (top right) along the same viewing direction, as well as similar representations along the-*b* axis. For the augmented nets, two-coordinated linkers are represented as solid lines and three-coordinated linkers as yellow triangles. The bismuth dimers are shown as distorted purple dodecahedra.

Crystal Structure of $Bi_6O_4(H_2TPTC)_5$ (5)

When performing synthesis in water using the tetracarboxylic acid H_4TPTC and $Bi(NO_3)_3 \cdot 5H_2O$, a coordination polymer was acquired, $Bi_6O_4(H_2TPTC)_5$ (**5**), as aggregates of stubby crystals (Figure S32). The structure was solved using cRED data from two individual crystals (Figure S33, Table S10) and subsequently refined against high-resolution XRPD data (Figure S34, Table S11). The IBU in **5** is that of a bismuth hexamer, containing four oxygen atoms acting as links between the Bi^{3+} ions of the cluster (Figure 11). The coordination number for bismuth in the structure is 6 and 7, with Bi-O bond distances ranging from 2.0 to 3.0 Å.

Regarding the topology, the clusters have high connectivities and are linked together by multiple two-, three-, and four-coordinated linker molecules. The framework can be simplified and represented as a (3,3,16)-c net (as shown in Figure 11). The bismuth hexamer is then 16-coordinated and is joined together by three-coordinated nodes representing either end of the H_2TPTC^{2-} ions. The acquired point symbol for this specific representation of **5** is $\{4.5^2\}_4\{4^{18}.5^{40}.6^{30}.7^{21}.8^{11}\}\{4^3.2\}$. The net does not form any natural tiling.

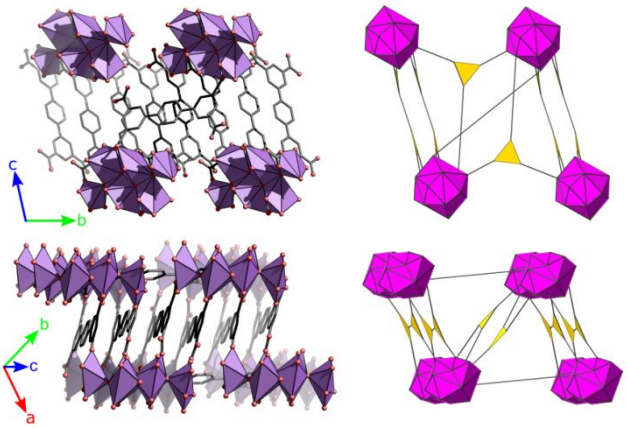

Figure 11. View along the *a*-axis for **5** (top left) and the corresponding augmented net (top right) along the same viewing direction, as well as similar representations viewed along the *c*-axis (bottom). The IBU of the structure is a bismuth hexamer, connected through H_2TPTC^{2-} ions, for which the branch points are represented as yellow triangles.

Conclusion

We have synthesized and characterized five bismuth coordination polymers, out of which one proved to be a breathing Bi-MOF. The five materials were characterized using a range of diffraction techniques, where three of the structures were solved using ED. The MOF SU-100 exhibits a solvent-dependent flexibility and undergoes reversible changes of up to 10.2 % of the unit cell volume, with a disproportionately large increase in solvent accessible void volume (26 %), depending on the solvent present. Upon heating the material and putting it in the ultra-high vacuum of a transmission electron microscope, the unit cell volume further expands (an increase of 21 %), whereas the solvent void volume decreases. Overall, the flexibility seems to originate in the inorganic building unit, a Bi_2O_{12} dimer, where the IBU contracts or expands, which in combination with the framework topology leads to significant changes in both unit cell volume and the volume of solvent-accessible voids inside the material. In the IBU of SU-100, the rhombus-shaped parts of the dimer seem to be a weak point of the structure, which, along with the existence of only even cycles in the **esg** net, help to promote the displacive transition that enables the breathing effect observed in the material.

SU-100 showed high uptake of CO_2 (3.09 mmol/g) and SF_6 (2.07 mmol/g) as well as high selectivity towards these gases. With a CO_2/N_2 selectivity of ~ 31 and a SF_6/N_2 selectivity of ~ 36, SU-100 could be a promising material for the separation and adsorption of greenhouse gases.

While isoreticular chemistry remains a challenge for Bi-MOFs and the chemistry of Bi^{3+} coordination polymers persistently remains unpredictable, structurally unique coordination polymers and MOFs are often acquired using bismuth. It is however expected that other reversibly flexible MOFs can be prepared using heavy cations, such as Bi^{3+}, with less distinct coordination geometries.

Experimental Section

All chemicals were purchased from Sigma-Aldrich or VWR International and used without further purification. All syntheses were carried out in sealed 5 mL borosilicate 3.3 glass tubes (Duran® 12 x 100 mm, DWK Life Sciences) certified for temperatures up to 180 °C, equipped with a polybutylene terephthalate (PBT) cap containing a PTFE seal. As the reactions were carried out under solvothermal conditions, care should be taken when reproducing any of the syntheses mentioned in this section, as high pressures are formed inside the reaction vessels and any scaling of the reactions should come with a proportionate scaling of the employed vessels.

High-resolution XRPD data for **1** (SU-100, as synthesized), **2**, and **5** were collected at 11BM at the Advanced Photon Source (APS), Argonne National Laboratory, USA, using the dedicated mail-in system. Additional high-resolution XRPD data, for DEF@SU-100, were gathered at ID22 at ESRF, Grenoble, France. In-house XRPD measurements were carried out using a Panalytical X'pert Pro diffractometer (Cu $K\alpha_{1,2}$, λ_1 = 1.540598 Å, λ_2 = 1.544426 Å) using a Bragg-Brentano geometry. SCXRD data were collected on a Bruker D8 Venture instrument equipped with a PHOTON 100 CMOS detector, using Mo Kα (λ = 0.71073 Å) radiation (**3** and **4**). Electron diffraction data were collected using a JEOL JEM2100 TEM, equipped with a Timepix detector from Amsterdam Scientific Instruments, while continuously rotating the crystal at 0.45° s^{-1}. For the SCXRD and 3D ED data, structure determination was performed using ShelXT.[44] Structure refinement against XRPD data was carried out using TOPAS-Academic V6.[45] For the SCXRD data, atomic positions and anisotropic displacement parameters were refined using a full-matrix least-squares technique against F^2 using ShelXL.[46] A riding model was used to constrain the coordinates of most hydrogen atoms bonded to carbon or oxygen atoms. Topological analyses of all framework structures were carried out using the software package ToposPro[47], as well as Systre[48] and 3dt (both part of the GAVROG package)[49].

Thermogravimetric analysis data were gathered using a Mettler Toledo TGA 2 and a TA Instruments Discovery TGA. Scanning electron microscopy images were collected on a JEOL JSM7401F SEM. Gas adsorption/desorption isotherms were recorded on a Micromeritics ASAP2020 surface area and porosity analyzer. Prior to the experiments, the samples were pretreated at 70 °C under dynamic vacuum (1 x 10^{-4} Pa) for 6 hours. Nitrogen (N_2) adsorption/desorption isotherms were recorded at liquid nitrogen temperature (-196 °C). A liquid N_2 bath was used as temperature control. The Langmuir and the Brunauer–Emmett–Teller (BET) specific surface area of SU-100 were calculated using the N_2 adsorption points recorded at a relative pressure range p/p_o = 0.05 – 0.15. Carbon dioxide (CO_2), nitrogen (N_2), sulfur hexafluoride (SF_6) and methane (CH_4) adsorption/desorption

isotherms were recorded at 0 °C. An ice slurry bath was used as the temperature control for these experiments.

Synthesis of SU-100 (1). The microporous framework SU-100 was prepared under solvothermal conditions by adding $Bi(NO_3)_3$•$5H_2O$ (20 mg), H_3BPT (15 mg) and methanol (3 mL) to a 5 mL glass tube equipped with a screw cap. The tube was sealed and heated at 160 °C for 1 hour in an Al heating block while stirring under autogenous pressure. The solid contents formed were then filtered off and the white powder (19 mg, 93 % yield with respect to Bi^{3+}) was left to dry without washing at room-temperature for 16 hours. Phase purity was confirmed by XRPD (Figure S4) and elemental analysis (calculated (%) for Bi(BPT)•2MeOH: C 36.71, H 2.72; measured (%): C 33.07 H 2.24).

MeOH@SU-100 was prepared by taking the as-synthesized SU-100 and immersing it in a small amount of methanol. When dry enough to behave like a powder, it was loaded into a Kapton capillary which was sealed with clay. DMF@SU-100 and DEF@SU-100 were prepared by heating 15 mg of SU-100 in 3 mL of DMF or DEF for one hour at 100 °C. The solid content was then filtered off and stored in sealed containers, prior to being loaded into capillaries for each respective measurement.

For the stability tests in various solvents, 20 mg of SU-100 was immersed in 3 mL of the solvent and stirred overnight at room temperature, before being filtered off and left to dry in ambient conditions.

Synthesis of 2. The coordination polymer Bi_2O_2(HBPT) was prepared under hydrothermal conditions by adding $Bi(NO_3)_3$•$5H_2O$ (25 mg), H_3BPT (15 mg) and de-ionized water (3 mL) to a 5 mL glass tube equipped with a screw cap. The tube was sealed and heated at 160 °C in an Al heating block for 1 hour while stirring under autogenous pressure, after which the solid contents where filtered off and the white powder (24 mg) was washed two times with 5 mL of N,N-dimethylformamide (DMF) to remove unreacted starting materials. The sample was then left to dry overnight. Phase purity was confirmed by XRPD (Figure S24) and elemental analysis (calculated (%) for Bi_2O_2(HBPT): C 24.54 H 1.10; measured (%): C 25.53 H 1.41).

Synthesis of 3. The coordination polymer $Bi(OH)(H_2BPT)_2$•$2H_2O$ was prepared (as a slight mixture with **2**) under hydrothermal conditions by adding $Bi(NO_3)_3$•$5H_2O$ (13 mg), H_3BPT (15 mg) and de-ionized water (3 mL) to a 5 mL glass tube equipped with a screw cap. The tube was sealed and heated at 120 °C in an Al heating block for 20 hours while stirring under autogenous pressure. The solid contents where then filtered off and left to dry overnight. The relative phase-purity could be determined by XRPD (Figure S29).

Synthesis of 4. The coordination polymer $Bi_2(HBPT)_3(H_2O)_3$•H_3BPT was acquired as large prismatic crystals by adding $Bi(NO_3)_3$•$5H_2O$ (25 mg), H_3BPT (15 mg) and de-ionized water (3 mL) to a 5 mL glass tube equipped with a screw cap, which was sealed and put in an oven at 120 °C for 7 days. The crystals of **4** could be isolated by washing the formed solid with 10 mL of hot DMF (70 °C), removing unreacted linker. The relative phase-purity could be confirmed by XRPD (Figure S31), yet the material was always acquired as a mixture.

Synthesis of 5. The coordination polymer $Bi_6O_4(H_2TPTC)_5$ was synthesized under hydrothermal conditions by mixing $Bi(NO_3)_3$•$5H_2O$ (24 mg), H_4TPTC (20 mg) and de-ionized water (2.5 mL) to a 5 mL glass tube equipped with a screw cap. The tube was sealed and heated at 160 °C in an Al heating block for 1 hour while stirring under autogenous pressure, after which the solid contents were filtered off and the white powder (16 mg) was left to dry overnight. Phase purity was confirmed by XRPD (Figure S34) and elemental analysis (calculated (%) for $Bi_6O_4(H_2TPTC)_5$: C 39.56 H 1.81; measured (%): C 37.22 H 1.83)

ASSOCIATED CONTENT

Crystallographic Information Files (CIFs), crystallographic tables, experimental and calculated XRPD patterns, SEM micrographs, thermodiffraction data, gas adsorption results, figures of solvent accessible voids and reciprocal space projections for ED data. This material is available free of charge via the Internet at http://pubs.acs.org.

CCDC 1926729-1926735 contains the supplementary crystallographic data for this paper. These data can be obtained free of charge via www.ccdc.cam.ac.uk/data_request/cif.

AUTHOR INFORMATION

Corresponding Author

* E-mail: andrew.inge@mmk.su.se
Telephone: +46 72 147 4427

Notes

The authors declare no competing financial interest.

ACKNOWLEDGMENTS

We thank Prof. Michael O'Keeffe for assistance in the topological analysis of the acquired metal-organic framework.

Use of the Advanced Photon Source at Argonne National Laboratory was supported by the U. S. Department of Energy, Office of Science, Office of Basic Energy Sciences, under Contract No. DE-AC02-06CH11357. E.S.G. and A.K.I. acknowledge support from the Swedish Foundation for Strategic Research (SFF). A.K.I. also acknowledges support from the Knut and Alice Wallenberg Foundation (KAW 2016.0072). O.C. acknowledges support from the Swedish Research Council for Sustainable Development (FOMAS, 2018-00651) and the Åforsk Foundation (19-549). D.M.P. thanks the Università degli Studi di Milano for the transition grant PSR2015-1718. X.Z. acknowledges support from the Swedish Research Council (VR, No. 2017-04321) as well as from the Knut and Alice Wallenberg Foundation through the project 3DEM-NATUR (KAW, No. 2012.0112).

REFERENCES

(1) Furukawa, H.; Cordova, K. E.; O'Keeffe, M.; Yaghi, O. M. The Chemistry and Applications of Metal-Organic Frameworks. *Science* **2013**, *341* (6149), 1230444.

(2) Schneemann, A.; Bon, V.; Schwedler, I.; Senkovska, I.; Kaskel, S.; Fischer, R. A. Flexible Metal–Organic Frameworks. *Chem. Soc. Rev.* **2014**, *43* (16), 6062–6096.

(3) Murdock, C. R.; Hughes, B. C.; Lu, Z.; Jenkins, D. M. Approaches for Synthesizing Breathing MOFs by Exploiting Dimensional Rigidity. *Coord. Chem. Rev.* **2014**, *258–259* (1), 119–136.

(4) Férey, G.; Serre, C. Large Breathing Effects in Three-Dimensional Porous Hybrid Matter: Facts, Analyses, Rules

and Consequences. *Chem. Soc. Rev.* **2009**, *38* (5), 1380–1399.

(5) Kitagawa, S.; Kitaura, R.; Noro, S. I. Functional Porous Coordination Polymers. *Angew. Chem. Int. Ed.* **2004**, *43* (18), 2334–2375.

(6) Serre, C.; Millange, F.; Thouvenot, C.; Noguès, M.; Marsolier, G.; Louër, D.; Férey, G. Very Large Breathing Effect in the First Nanoporous Chromium(III)-Based Solids: MIL-53 or CrIII(OH)·{O2C-C6H4- CO2}·{HO2C-C6H4 - CO2H}x·H2Oy. *J. Am. Chem. Soc.* **2002**, *124* (45), 13519–13526.

(7) Sarkisov, L.; Martin, R. L.; Haranczyk, M.; Smit, B. On the Flexibility of Metal-Organic Frameworks. *J. Am. Chem. Soc.* **2014**, *136* (6), 2228–2231.

(8) Chen, Y.; Zhang, J.; Li, J.; Lockard, J. V. Monitoring the Activation of a Flexible Metal-Organic Framework Using Structurally Sensitive Spectroscopy Techniques. *J. Phys. Chem. C* **2013**, *117* (39), 20068–20077.

(9) Bon, V.; Senkovska, I.; Wallacher, D.; Többens, D. M.; Zizak, I.; Feyerherm, R.; Mueller, U.; Kaskel, S. In Situ Observation of Gating Phenomena in the Flexible Porous Coordination Polymer Zn2(BPnDC)2(Bpy) (SNU-9) in a Combined Diffraction and Gas Adsorption Experiment. *Inorg. Chem.* **2014**, *53* (3), 1513–1520.

(10) Schneemann, A.; Vervoorts, P.; Hante, I.; Tu, M.; Wannapaiboon, S.; Sternemann, C.; Paulus, M.; Wieland, D. C. F.; Henke, S.; Fischer, R. A. Different Breathing Mechanisms in Flexible Pillared-Layered Metal-Organic Frameworks: Impact of the Metal Center. *Chem. Mater.* **2018**, *30* (5), 1667–1676.

(11) De Marcillac, P.; Coron, N.; Dambier, G.; Leblanc, J.; Moalic, J. P. Experimental Detection of α-Particles from the Radioactive Decay of Natural Bismuth. *Nature* **2003**, *422* (6934), 876–878.

(12) Feyand, M.; Mugnaioli, E.; Vermoortele, F.; Bueken, B.; Dieterich, J. M.; Reimer, T.; Kolb, U.; De Vos, D.; Stock, N. Automated Diffraction Tomography for the Structure Elucidation of Twinned, Sub-Micrometer Crystals of a Highly Porous, Catalytically Active Bismuth Metal-Organic Framework. *Angew. Chem. Int. Ed.* **2012**, *51* (41), 10373–10376.

(13) Savage, M.; Yang, S.; Suyetin, M.; Bichoutskaia, E.; Lewis, W.; Blake, A. J.; Barnett, S. A.; Schröder, M. A Novel Bismuth-Based Metal-Organic Framework for High Volumetric Methane and Carbon Dioxide Adsorption. *Chem. Eur. J.* **2014**, *20* (26), 8024–8029.

(14) Inge, A. K.; Köppen, M.; Su, J.; Feyand, M.; Xu, H.; Zou, X.; O'Keeffe, M.; Stock, N. Unprecedented Topological Complexity in a Metal-Organic Framework Constructed from Simple Building Units. *J. Am. Chem. Soc.* **2016**, *138* (6), 1970–1976.

(15) Köppen, M.; Meyer, V.; Ångström, J.; Inge, A. K.; Stock, N. Solvent-Dependent Formation of Three New Bi-Metal-Organic Frameworks Using a Tetracarboxylic Acid. *Cryst. Growth Des.* **2018**, *18* (7), 4060–4067.

(16) Robison, L.; Zhang, L.; Drout, R. J.; Li, P.; Haney, C. R.; Brikha, A.; Noh, H.; Mehdi, B. L.; Browning, N. D.; Dravid, V. P.; et al. A Bismuth Metal–Organic Framework as a Contrast Agent for X-Ray Computed Tomography. *ACS Appl. Bio Mater.* **2019**, *2*, 1197–1203.

(17) Keogan, D. M.; Griffith, D. M. Current and Potential Applications of Bismuth-Based Drugs. *Molecules* **2014**, *19* (9), 15258–15297.

(18) Li, H.; Sun, H. Recent Advances in Bioinorganic Chemistry of Bismuth. *Curr. Opin. Chem. Biol.* **2012**, *16* (1–2), 74–83.

(19) Sadler, P. J.; Li, H.; Sun, H. Coordination Chemistry of Metals in Medicine: Target Sites for Bismuth. *Coord. Chem. Rev.* **1999**, *185–186*, 689–709.

(20) Hong, Y.; Lai, Y.-T.; Chan, G. C.-F.; Sun, H. Glutathione and Multidrug Resistance Protein Transporter Mediate a Self-Propelled Disposal of Bismuth in Human Cells. *Proc. Natl. Acad. Sci.* **2015**, *112* (11), 3211–3216.

(21) Wang, R.; Lai, T. P.; Gao, P.; Zhang, H.; Ho, P. L.; Woo, P. C. Y.; Ma, G.; Kao, R. Y. T.; Li, H.; Sun, H. Bismuth Antimicrobial Drugs Serve as Broad-Spectrum Metallo-β-Lactamase Inhibitors. *Nat. Commun.* **2018**, *9* (1), 439.

(22) Wang, Y.; Takki, S.; Cheung, O.; Xu, H.; Wan, W.; Öhrström, L.; Inge, A. K. Elucidation of the Elusive Structure and Formula of the Active Pharmaceutical Ingredient Bismuth Subgallate by Continuous Rotation Electron Diffraction. *Chem. Commun.* **2017**, *53* (52), 7018–7021.

(23) Nederlof, I.; van Genderen, E.; Li, Y.-W.; Abrahams, J. P. A Medipix Quantum Area Detector Allows Rotation Electron Diffraction Data Collection from Submicrometre Three-Dimensional Protein Crystals. *Acta Crystallogr. Sect. D Biol. Crystallogr.* **2013**, *69* (7), 1223–1230.

(24) Shi, D.; Nannenga, B. L.; Iadanza, M. G.; Gonen, T. Three-Dimensional Electron Crystallography of Protein Microcrystals. *Elife* **2013**, *2* (e01345).

(25) Xu, H.; Lebrette, H.; Hovmöller, S.; Högbom, M.; Srinivas, V.; Yang, T.; Zou, X. A Rare Lysozyme Crystal Form Solved Using Highly Redundant Multiple Electron Diffraction Datasets from Micron-Sized Crystals. *Structure* **2018**, *26* (4), 667-675.e3.

(26) Wang, B.; Rhauderwiek, T.; Inge, A. K.; Xu, H.; Yang, T.; Huang, Z.; Stock, N.; Zou, X. A Porous Cobalt Tetraphosphonate Metal-Organic Framework: Accurate Structure and Guest Molecule Location Determined by Continuous-Rotation Electron Diffraction. *Chem. Eur. J.* **2018**, *24* (66), 17429–17433.

(27) Mugnaioli, E.; Gorelik, T.; Kolb, U. "Ab Initio" Structure Solution from Electron Diffraction Data Obtained by a Combination of Automated Diffraction Tomography and Precession Technique. *Ultramicroscopy* **2009**, *109* (6), 758–765.

(28) Kolb, U.; Krysiak, Y.; Plana-Ruiz, S. Automated Electron Diffraction Tomography – Development and Applications. *Acta Crystallogr. Sect. B Struct. Sci. Cryst. Eng. Mater.* **2019**, *75* (4), 463–474.

(29) Nannenga, B. L.; Shi, D.; Leslie, A. G. W.; Gonen, T. High-Resolution Structure Determination by Continuous-Rotation Data Collection in MicroED. *Nat. Methods* **2014**, *11* (9), 927.

(30) Keeffe, M. O.; Peskov, M. A.; Ramsden, S. J.; Yaghi, O. M. The Reticular Chemistry Structure Resource (RCSR) database of, and symbols for, crystal nets. *Acc. Chem. Res.* **2008**, *41* (12), 1782-1789.

(31) Chesnut, D. J.; Plewak, D.; Zubieta, J. Solid State Coordination Chemistry of the Copper(I)-Cyano-Organodiimine System. Two- and Three-Dimensional Copper Cyanide Phases Incorporating Linear Dipodal Ligands. *J. Chem. Soc. Dalt. Trans.* **2001**, *18*, 2567–2580.

(32) Blatov, V. A.; Proserpio, D. M. Topological Relations between Three-Periodic Nets. II. Binodal Nets. *Acta Crystallogr. Sect. A Found. Crystallogr.* **2009**, *65* (3), 202–212.

(33) Song, S. Y.; Song, X. Z.; Zhao, S. N.; Qin, C.; Su, S. Q.; Zhu, M.; Hao, Z. M.; Zhang, H. J. Syntheses, Structures and Physical Properties of Transition Metal-Organic Frameworks Assembled from Trigonal Heterofunctional Ligands. *Dalt. Trans.* **2012**, *41*, 10412.

(34) Spek, A. L. Structure Validation in Chemical Crystallography. *Acta Crystallogr. Sect. D Biol. Crystallogr.* **2009**, *65* (2), 148–155.

(35) Choi, S.; Drese, J. H.; Jones, C. W. Adsorbent Materials for Carbon Dioxide Capture from Large Anthropogenic Point Sources. *ChemSusChem* **2009**, *2* (9), 796–854.

(36) Cheung, O.; Hedin, N. Zeolites and Related Sorbents with Narrow Pores for CO_2 Separation from Flue Gas. *RSC Adv.* **2014**, *4* (28), 14480–14494.

(37) Sumida, K.; Rogow, D. L.; Mason, J. A.; McDonald, T. M.; Bloch, E. D.; Herm, Z. R.; Bae, T. H.; Long, J. R. Carbon Dioxide Capture in Metal-Organic Frameworks. *Chem. Rev.* **2012**, *112* (2), 724–781.

(38) Liu, Q.; Cheung, N. C. O.; Garcia-Bennett, A. E.; Hedin, N. Aluminophosphates for CO_2 Separation. *ChemSusChem* **2011**, *4* (1), 91–97.

(39) Cheung, O.; Bacsik, Z.; Liu, Q.; Mace, A.; Hedin, N. Adsorption Kinetics for CO_2 on Highly Selective Zeolites NaKA and Nano-NaKA. *Appl. Energy* **2013**, *112*, 1326–1336.

(40) Cheung, O.; Liu, Q.; Bacsik, Z.; Hedin, N. Silicoaluminophosphates as CO_2-Sorbents. *Microporous Mesoporous Mater.* **2012**, *156*, 90–96.

(41) Christophorou, L. G.; Van Brunt, R. J. SF6/N2Mixtures Basic and HV Insulation Properties. *IEEE Trans. Dielectr. Electr. Insul.* **1995**, *2* (5), 952–1003.

(42) Solomon, S.; Qin, D.; Manning, M.; Averyt, K.; Marquis, M. *Climate Change 2007 - The Physical Science Basis: Working Group I Contribution to the Fourth Assessment Report of the IPCC*; 2007.

(43) Rosi, N. L.; Kim, J.; Eddaoudi, M.; Chen, B.; O'Keeffe, M.; Yaghi, O. M. Rod Packings and Metal-Organic Frameworks Constructed from Rod-Shaped Secondary Building Units. *J. Am. Chem. Soc.* **2005**, *127* (5), 1504–1518.

(44) Sheldrick, G. M. SHELXT - Integrated Space-Group and Crystal-Structure Determination. *Acta Crystallogr. Sect. A* **2015**, *71* (1), 3–8.

(45) Coelho, A. TOPAS-Academic V6. Coelho Software 2016.

(46) Sheldrick, G. M. A Short History of SHELX. *Acta Crystallogr. Sect. A Found. Crystallogr.* **2008**, *64* (1), 112–122.

(47) Blatov, V. A.; Shevchenko, A. P.; Proserpio, D. M. Applied Topological Analysis of Crystal Structures with the Program Package ToposPro. *Cryst. Growth Des.* **2014**, *14* (7), 3576–3586.

(48) Delgado-Friedrichs, O.; O'Keeffe, M. Identification of and Symmetry Computation for Crystal Nets. *Acta Crystallogr. Sect. A Found. Crystallogr.* **2003**, *59* (4), 351–360.

(49) Delgado-Friedrichs, O. The GAVROG Project (2017) http://www.gavrog.org/.

Insert Table of Contents artwork here

For Table of Contents Use Only

A Breathing Metal-Organic Framework Based on Flexible Inorganic Building Units

Erik Svensson Grape, Hongyi Xu, Ocean Cheung, Marion Calmels, Jingjing Zhao, Catherine Dejoie, Davide M. Proserpio, Xiaodong Zou, A. Ken Inge

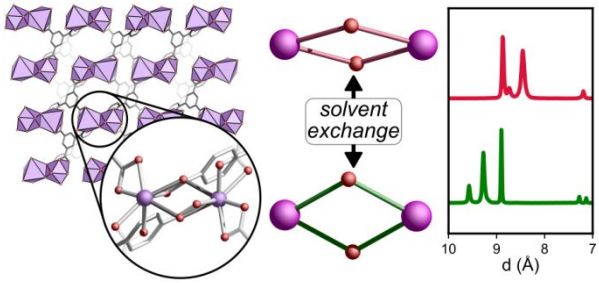

A breathing metal-organic framework was synthesized from Bi^{3+} cations. The structure adapts to various solvent molecules introduced as guest species. Flexibility of the overall framework is attributed to flexible inorganic building units, as changes were observed in the coordination geometry of the Bi^{3+} cations.